

先進閘極介電層互補式金氧半電晶體中電壓溫度引致不穩定性之研究

學生：詹前泰

指導教授：汪大暉博士

國立交通大學 電子工程學系 電子研究所

摘 要

本論文提出一新穎之量測方法，並據以研究先進閘極介電層互補式金氧半電晶體中電壓溫度引致之不穩定性。此方法包括一自行組裝之電腦自動化量測電路系統，以及特殊設計之實驗技巧。傳統量測方法於加壓與量測之間，存在大約數秒之延遲，期間發生的電荷散逸將嚴重影響實驗數據的可信度與完整性。本論文所提之創新方法可有效縮短延遲至數微秒，成功攫取暫態訊號，發現新的現象並得以研究其物理。

第二章詳述此新穎量測電路之各零組件、系統效能、並展示於實際 CMOS 元件以及記憶體元件測試之量測結果。第三章介紹應用第二章所提之電路所發展之實驗方法—「暫態回復技巧」。此法之理論基礎與實際應用都將詳列於此章。吾人發現，經電壓溫度加壓，大面積元件具有可觀之回復效應；回復過程中，汲極電流對時間呈現 log 關係。同樣地，小面積元件亦有回復現象，但其汲極電流對時間的關係，則以不連續的、階梯式的圖像呈現。吾人研究發現，此量子化行為，乃一顆一顆儲存於介電層缺陷中的電荷散逸所致。藉由研究電場以及溫度對單電荷散逸之影響，吾人提出一可解析之物理模型—「熱助穿隧」，成功地解釋所得之實驗結果。此模型配合實驗結果，可進一步粹取缺陷特性，如活化能以及缺陷密度等等。最後，吾人以此方法比較不同閘極材料中缺陷的特性之異同。

第四章探討 HfSiON nMOSFETs 中正電壓溫度所引致之不穩定性 (PBTI)。有別於傳統量測，本研究以第二章所述之量測方法發現，延遲轉換將嚴重低估 PBTI 所造成的退化量。吾人實驗結果發現 PBTI 引致之汲極電流退化呈現兩階段 (two-stage degradation) 發展。第一個階段由填補初始缺陷 (initial trap filling) 主導退化，具 log 時間關係並與溫度呈現負相關。第二階段，額外缺陷產生 (additional trap generation) 的效應將超越初始缺陷填補，成為退化主因；此階段與時間成指數 (power-law) 關係並與溫度成正相關。此外，吾人利用第二章所提之單電荷散逸量測和暫態回復技巧、輔以常用的電荷幫浦 (charge pumping) 法所得之實驗結果，與前述退化模型相呼應。最後評估的是製程對缺

陷產生以及兩階段退化特性的影響。

第五章研究 HfSiON pMOSFETs 中負電壓溫度所引致之不穩定性(NBTI)。低電壓或者室溫加壓，汲極電流退化的現象與一般預期無異：隨加壓時間呈現一路退化的趨勢、增加電壓強度或溫度則退化更嚴重。但再升高電壓或溫度，吾人則觀察到汲極電流隨時間之變化呈現奇特的「轉彎現象」(turn-around)：一開始汲極電流增加，到某時間點增加至最大值後開始降低，其後便一路減少並回歸到電流退化。愈高電壓以及愈高溫度下愈明顯。在本研究所有實驗條件下，在 10 秒以前汲極電流都會進入退化，所以一般量測方法若是忽略暫態效應，將無法清楚地觀測到此特殊現象。吾人提出一「雙極電荷模型」成功解釋實驗結果，並再次以單電荷散逸量測、以及電荷幫浦法，驗證所提出之物理模型。

最後於第六章，吾人總結本論文之貢獻，並提出未來研究方向的建議。

關鍵字：互補式金氧半電晶體，可靠度，高介電閘極氧化層，正電壓溫度引致不穩定性，負電壓溫度引致不穩定，回復，暫態量測，單電荷散逸，缺陷特性，兩階段退化，雙極電荷模型



Bias Temperature Instability in CMOSFETs with Advanced Gate Dielectrics

Student : Chien-Tai Chan

Advisor : Dr. Tahui Wang

Department of Electronics Engineering & Institute of Electronics
National Chiao Tung University

ABSTRACT

This thesis proposes a novel characterization methodology to study the bias temperature instability (BTI) in advanced gate dielectrics (mainly high-k) for CMOS technology. The methodology includes a computer-automated measurement circuit system and specially-designed experimental techniques. The system minimizes the switching delay between stress and measurement down to $\sim\mu\text{s}$, and successfully retrieves the valuable information which has been ignored in a conventional method where during the switching delay significant charge de-trapping takes place.

The components, capabilities, and demonstrations of the proposed transient measurement system are described in detail in Chapter 2. In Chapter 3, a novel recovery transient technique involving direct measurement of single charge phenomena is presented. Both large- and small-area MOSFETs are characterized. In a large-area device, the post-BTI drain current exhibits a recovery transient and follows logarithmic time dependence. In a small-area device, individual trapped charge emission from gate dielectric traps is observed during recovery, which is manifested by a staircase-like drain current evolution with time. By measuring the effects of electric field and temperature on the charge emission times, one can identify the physical mechanism for charge escape. An analytical model based on thermally assisted tunneling can successfully reproduce measured transient characteristics. One can also extract trap properties such as the activation energy and the trap density. Applications of the technique to comparison between different gate dielectric materials are also demonstrated.

Drain current degradation in HfSiON gate dielectric nMOSFETs due to positive bias and temperature (PBT) stress is investigated in Chapter 4 by using the fast transient measurement system introduced in Chapter 2. The degradation exhibits two stages, featuring different degradation rates and stress temperature dependence. The first stage degradation is attributed to charging of the pre-existing high-k dielectric traps and has $\log(t)$ dependence on stress time and negative temperature dependence while the second stage degradation is mainly caused by new high-k trap creation following a power-law time relation and positive temperature dependence. The high-k trap growth rate is characterized by two techniques, the recovery transient technique proposed in Chapter 3 and the well-known charge pumping technique. Finally, the impact of processing on high-k trap growth is evaluated.

In Chapter 5, negative bias temperature instability (NBTI) is explored for pMOSFET's with HfSiON as the high-k gate dielectric. An anomalous turn-around in NBT stress induced drain current change is observed. For low stress gate voltage amplitude ($|V_g|$) and/or low temperature, the drain current degrades with time and increase in stress strength aggravates the degradation. Further increase in ($|V_g|$) and/or in temperature, in contrast, leads to an anomalous turn-around in the temporal evolution of drain current. The drain current initially enhances, reaches a peak, goes downhill, and eventually enters degradation. The phenomenon occurs within 10 seconds for most stress conditions in this work, and thus is easily neglected in a conventional method. The measured enhancement grows with increasing stress $|V_g|$ and temperature. A physical model incorporating bipolar charge trapping is proposed to account for the experimental results. Direct measurement of single charge de-trapping and charge pumping measurement are performed and the results justify the model.

Finally, the contributions of this dissertation are summarized and the directions for the future works are suggested in Chapter 6.

Keyword: CMOS Reliability, High-k, PBTI, NBTI, Recovery, Transient Measurement, Single Charge Emission, Trap Properties, Two Stage Degradation, Bipolar Charging Model

ACKNOWLEDGEMENT

I would like to express my deepest gratitude to my supervisor, Prof. Tahui Wang for his constant guidance and encouragement throughout the course of study.

I also show my appreciation to all of the committee members for their invaluable comments and suggestions. Moreover, I would like to acknowledge Dr. Howard C.-H. Wang, Dr. Ching-Wei Tsai, and Dr. Shang-Jr Chen at TSMC for providing cutting-edge devices and comments from industry's viewpoints.

From undergraduate to graduate study, many professors have influenced or encouraged me in research and in philosophy of life. Among them, I would like to thank Prof. Steve S. Chung, Prof. Min-Jer Chen, Prof. Tiao-Yuan Huang, Prof. Chien-Ping Lee, and Prof. Jung Tsai. Also, I would like to express my appreciation to the President of NCTU, Dr. Chun-Yen Chang, and the Dean of College of EECS, Dr. Chung-Yu Wu, for their recommendation for travel grant from Foundation for the Advancement of Outstanding Scholarship for outstanding students.

During the almost seven-year-long period, I enjoy very much working with all the members in the Emerging Devices and Technology Lab. In particular, I would like to thank Dr. Ching-Wei Tsai, Dr. Min-Cheng Chen, and Dr. Jun-Wei Wu for their guidance during my initial stage of Ph. D. study; special thanks are also given to Mr. Shau-Hong Ku, Mr. Hsin-Kai Chiang, Mr. Chih-Chang Cheng, Mr. Huan-Chi Ma, and Mr. Chun-Jung Tang for the fun time we spent together in the lab. The assistance in executing routine measurements from Mr. Chun-Jung Tang, Mr. Jian-Wen You, and Mr. Jin-Hau Kuo is also greatly appreciated.

Scholarship from the Chung Hwa Rotary Educational Foundation as recommended by Taoyuan Fu-Hsing Rotary Club (District 3500) is deeply acknowledged for easing my financial pressure. I would like to appreciate as well the Foundation for the Advancement of Outstanding Scholarship, the Yen Tjing Ling Industrial Research Institute, and National Science Council for providing the travel grants for me to present papers in international conferences.

Last but not least, the love from my family and Mrs. Ssu-Ying Chen is always the most important support for me. This dissertation is dedicated to them.

謝誌

首先，感謝指導教授汪大暉博士。從大學部專題加入研究群至今將近七年的時間，在學術上，老師無私的指導以及做研究嚴謹的態度，將使我受用一生；研究初期不甚順遂，老師亦時時給予鼓勵與建議，方能堅持到學位的完成。沒有汪老師的教誨與支持，這本論文將無法完成。

特別感謝論文口試委員在百忙之中給予寶貴的建議與指教。另外，台灣積體電路製造公司經理王志豪博士、蔡慶威博士、以及陳尚志博士在元件的製備和提供上大力協助，在此亦表達由衷的感謝。

在交大求學過程中，課業以及生涯規劃受教於電子系莊紹勳教授、陳明哲教授、黃調元教授、李建平教授和已退休的蔡中教授；申請傑出人才基金會(Foundation for the Advancement of Outstanding Scholarship)優秀學生出國補助時，幫我寫推薦函的校長張俊彥博士和電機資訊學院院長吳重雨博士，在此也表達我的感謝。

感謝學長蔡慶威博士、陳旻政博士以及吳俊威博士不吝分享所學，讓我快速進入狀況；感謝同在攻讀博士學位的古紹泓先生、江欣凱先生、鄭志昌先生、馬煥淇先生以及唐俊榮先生在實驗室和我一起討論、一起受挫、也一起分享喜悅，這段時光將是我人生中美好的一段回憶，也祝他們順利畢業。此外，感謝唐俊榮先生、游建文先生、以及郭晉豪先生分擔實驗的工作；也感謝前瞻元件與技術實驗室所有成員，他們為我的博士班生涯增色許多。

感謝財團法人中華扶輪教育基金會提供獎學金(Scholarship of the Chung Hwa Rotary Educational Foundation)，減輕我的經濟壓力；亦在此向推薦我的3500地區桃園福興扶輪社和時任社長的楊如松先生致上誠摯的謝意。感謝財團法人傑出人才發展基金會(Foundation for the Advancement of Outstanding Scholarship)、台大嚴慶齡工業研究中心(Yen Tjing Ling Industrial Research Institute)、以及國科會(National Science Council)，提供經費補助讓我前往國際會議發表論文。

最後，我要感謝長久以來支持我的家人和女友思穎，他們的愛是我的重要支柱。這本論文，獻給他們。

CONTENTS

Chinese Abstract		i
English Abstract		iii
Acknowledgement		v
Contents		vii
Table Captions		ix
Figure Captions		x
List of Symbols		xvi
Chapter 1	Introduction	1
1.1	Backgrounds	1
1.2	Description of the Problem	3
1.3	Organization of the Dissertation	4
Chapter 2	A Fast -Transient Measurement System and Experimental Techniques	9
2.1	Necessity of Transient Measurement	9
2.2	Existing Techniques	10
	2.2.1 RF Kits	10
	2.2.2 Series Resistance	11
	2.2.3 Operational Amplifiers	12
2.3	A Computer-Automated Measurement System	12
	2.3.1 The System	12
	2.3.2 System Capability	13
2.4	Summary	14
Chapter 3	Single Charge Emission: A Novel Technique to Investigate Trap Properties in Advanced Gate Dielectrics	25
3.1	Preface	25
3.2	Recovery Transient Measurement	26
	3.2.1 Experimental	26
	3.2.2 Recovery Transient in Large-Area Devices	27
	3.2.3 Single Electron Emission in Small-Area Devices	28
3.3	Results and Discussions	29
	3.3.1 The Trapped Charge Emission Model	29
	3.3.2 High-k Trap Density	31
	3.3.3 Modeling of Recovery Transient in Large-Area Devices	32
	3.3.4 Gate Length Effect	36
3.4	Applications of the Technique	36
	3.4.1 Study of NBTI in SiO ₂ pMOSFETs	36

	3.4.2	Comparison between High-k and SiO ₂	37
3.5		Summary	38
Chapter 4		Characteristics and Physical Mechanisms of Positive Bias and Temperature Stress Induced Drain Current Degradation in HfSiON nMOSFETs	57
4.1		Preface	57
4.2		Devices	58
4.3		Two-Phase Measurement	58
4.4		Results and Discussions	59
	4.4.1	Two-Stage Drain Current Degradation	59
	4.4.2	The Degradation Model	60
	4.4.3	High-k Trap Growth Rate	61
	4.4.4	The Impact of Processing	65
4.5		Summary	66
Chapter 5		Negative Bias Temperature Instability in High-k pMOSFETs	88
5.1		Preface	88
5.2		Devices	89
5.3		Anomalous Turn-Around in Drain Current Degradation	89
5.4		The Bipolar Charging Model	90
5.5		Charge Pumping and Single Charge Emission	92
5.6		Impact of High-k Integrity	93
5.7		Summary	94
Chapter 6		Conclusions	109
6.1		Summary of Contributions	109
6.2		Suggestions for Future Works	110
References			111
Vita			125
Publication List			126

TABLE CAPTIONS

Chapter 3

- Table 3.1 Summary of E_a , τ_1 , amplitude of the current jumps (ΔI_d), τ_2/τ_1 , and the calculated N_t for high-k nMOS, high-k pMOS, and SiO₂ pMOS devices.
- Table 3.2 Summary of the values used in the text.

Chapter 5

- Table 5.1 Summary of dominant degradation mechanisms under various stress conditions. Detailed discussions are given in the text.



FIGURE CAPTIONS

Chapter 1

- Fig. 1.1 Projections of gate leakage current and equivalent oxide thickness (EOT) from ITRS roadmap for high-performance (a) and low-standby-power (b) applications.
- Fig. 1.2 Summary of high-k materials being studied. Data quoted from [1.15].
- Fig. 1.3 The organization of the dissertation.

Chapter 2

- Fig. 2.1 The operating principles of a conventional measurement method in characterization of non-volatile memories (a) and of CMOS devices (b).
- Fig. 2.2 Energy band diagrams during stressing or programming (a) and during measurement (b). Charge de-trapping may take place during measurement.
- Fig. 2.3 The measurement setup including components with radio frequency response for self-heating free characterization in SOI devices proposed in [2.1].
- Fig. 2.4 The pulse-IV measurement setup incorporating a series resistance proposed in [2.3].
- Fig. 2.5 The measurement setup using an operational amplifier proposed in [2.4].
- Fig. 2.6 (a) This work, in addition to the operational amplifier, takes advantage of high-speed analog switches to minimize the switching delay down to μs . (b) The waveforms for transient measurement.
- Fig. 2.7 The image of the transient measurement circuit.
- Fig. 2.8 Recovery transient in a high-k nMOS device. As clearly shown, significant charge de-trapping occurs in sub-second regime. Detailed physics will be discussed in the following chapters.
- Fig. 2.9 Program state retention characteristics spanning eight decades of time.

Chapter 3

- Fig. 3.1 (a) Schematic diagram for PBTI recovery transient measurement. (b) The waveforms applied to the gate and drain during stress and recovery phases.

- Fig. 3.2 Temporal evolutions of the drain current before and after stress in a nMOSFET with SiO₂ as the gate dielectric, measured by the experimental setup in Fig. 3.1.
- Fig. 3.3 Temporal evolutions of the drain current before and after stress in a large area high-k nMOSFET. $V_g=0.7V$, 0.2s for stress and $V_g/V_d=0.1V/0.2V$ for recovery. The device dimension is $W/L=100\mu m/0.08\mu m$. The symbols represent measurement data and the line calculation.
- Fig. 3.4 Recovery drain current transients before and after stress in a small-area device. The bias condition for stress is the same as in Fig. 3.3, and for recovery $V_g/V_d=0.3V/0.2V$. The device dimension is $W/L=0.16\mu m/0.08\mu m$. Each current jump is attributed to single trapped charge escape from high-k gate dielectric. Only three electrons are trapped during stress. The emission time of the three trapped electrons is denoted as τ_1 , τ_2 , and τ_3 .
- Fig. 3.5 Temperature dependence of $\langle \tau_1 \rangle$. The activation energy extracted from the Arrhenius plot is 0.18eV. Each data point is an average of ten readings.
- Fig. 3.6 Dependence of trapped electron emission times on recovery gate voltage. Ten measurements are made for each recovery V_g to take average.
- Fig. 3.7 The energy band diagram illustrating possible paths for trapped charge emission: (a) Frenkel-Poole (FP) emission, (b) tunneling to the gate, and (c) tunneling to the Si substrate.
- Fig. 3.8 The energy band diagram corresponding to the stress condition where $V_g=0.7V$ is applied to inject electron into the high-k traps.
- Fig. 3.9 Schematic representation of the band diagram in recovery phase and trap positions. E_a is the activation energy for SRH-like thermally assisted tunneling (TAT).
- Fig. 3.10 The ratio of τ_2 to τ_1 versus gate voltage in recovery phase. Note that τ_2/τ_1 remains almost unchanged with respect to V_g , as predicted by Eq. (3.3). The extracted high-k trap density is $3.5 \times 10^{17} \text{cm}^{-3}$, or equivalently $8.8 \times 10^{10} \text{cm}^{-2}$.
- Fig. 3.11 Normalized drain current evolution with recovery time for two stress V_g 's (0.7V and 1V). The V_g in recovery phase is 0.1V.
- Fig. 3.12 (a) Comparison of the current jump amplitude for $L_{\text{gate}}=0.14\mu m$ and $L_{\text{gate}}=$

0.08 μ m. Both devices are subject to identical stress and recovery conditions.

(b) The amplitude of the current jump versus L_{gate} .

Fig. 3.13 (a) A typical step-like “quantum jump” observed in channel current during NBTI recovery in a SiO₂ pMOSFET. (b) Compared to a “weak stress” condition ($V_g = -3V, 2s$) in (a) in which only two quantum jumps are measured, a post “strong stress” ($V_g = -3V, 300s$) recovery has five jumps in the same time window.

Fig. 3.14 Comparison of the staircase-like current jumps for a (a) high-k nMOS, (b) high-k pMOS, and (c) SiO₂ pMOS device.

Fig. 3.15 Comparison of the recovery V_g dependence of charge emission times for a (a) high-k nMOS, (b) high-k pMOS, and (c) SiO₂ pMOS device.

Fig. 3.16 Comparison of the temperature dependence of the first charge emission time. The activation energy E_a is extracted to be (a) 0.18eV for high-k nMOS, (b) 0.14eV for high-k pMOS, and (c) 0.5eV for SiO₂ pMOS device.

Chapter 4

Fig. 4.1 (a) Setup for fast transient measurement as described in Chapter 2. (b) Pulses applied to gate and drain for stress and measurement. The stress time (t_{stress}) is scheduled on a log-time base and the stress gate voltage ($V_{g, stress}$) varies. The measurement condition is $V_{g, meas} = 1.2V$ and $V_{d, meas} = 0.2V$. A measurement time (t_{meas}) of 50 μs is chosen such that it is long enough to integrate signals reliably and short enough to avoid additional degradation.

Fig. 4.2 Linear drain current degradation as a result of PBTI stress at $V_g = 2.2V$ and $2.4V, T = 100C$. Two-stage degradation is observed. The onset time of the accelerated degradation is denoted by τ_c (corner time). The first stage degradation is the degradation before τ_c , and the second stage is after τ_c .

Fig. 4.3 The drain current degradation rate in the first stage (a) and in the second stage (b). The second stage degradation is obtained by subtracting the extrapolation of the first stage degradation from the measured ΔI_d .

Fig. 4.4 Stress temperature effect on I_d degradation for $V_g = 1.8V$ (a) and $2.2V$ (b). A cross-over of the I_d degradation at $T = 25C$ and $125C$ is noticed and a larger stress V_g gives an earlier crossover.

- Fig. 4.5 The corner time τ_c versus stress V_g at $T=25C$ and $125C$. The I_d degradation is driven into the second stage earlier (a smaller τ_c) at a higher stress V_g and temperature.
- Fig. 4.6 The characterization procedure of the two methods for high-k trap density extraction. (a) A drain current recovery transient technique. (b) A two-frequency charge pumping technique.
- Fig. 4.7 Drain current recovery transients measured at $V_g/V_d=0.25V/0.1V$ in a fresh and in a post-2000s-PBTI-stressed device.
- Fig. 4.8 Normalized drain current recovery transients measured at $V_g/V_d=0.25V/0.1V$ for different PBTI stress times: $t=0s$, $1s$, and $2000s$. Devices dimension is $W/L=100\mu m/0.08\mu m$. The increased slope implies additional traps are generated during stress.
- Fig. 4.9 The energy band diagram illustrating high-k trapped charge de-trapping during drain current recovery transient.
- Fig. 4.10 The pre- and post-stress I_d-V_g characteristics in a linear scale (a) and in a semi-log scale (b).
- Fig. 4.11 High-k trap density versus stress time from the recovery transient technique. The trap density is normalized to the initial high-k trap density.
- Fig. 4.12 Drain current recovery transient in a small-area device with $W/L=0.16\mu m/0.08\mu m$: (a) for stress time= $0s$ only one current jump is observed, and (b) after stress at $V_g=3V$, $T=100C$ for $100s$, up to five current jumps are presented. The increase in the number of current jumps indicates additional traps are created during stress.
- Fig. 4.13 High-k trap density versus stress time from the CP technique. The trap density is normalized to the initial high-k trap density. (a) Stress temperature= $25C$, (b) stress gate voltage= $2V$.
- Fig. 4.14 Generated high-k trap density versus stress time from the recovery transient and the CP techniques. The stress condition is $V_g=2.2V$, $T=25C$.
- Fig. 4.15 Comparison of BTI-limited lifetime between the “optimal” and the “control” devices [4.2]. The BTI measurements are performed by using a conventional characterization method.
- Fig. 4.16 Comparison of hot carrier injection limited lifetime between the “optimal”

and the “control” devices [4.2]. The measurements are performed by using a conventional characterization method.

- Fig. 4.17 Comparison of time-to-breakdown between the “optimal” and the “control” devices [4.2].
- Fig. 4.18 PBTI stress robustness of two devices: “optimal” vs. “control.” While both have an identical transfer characteristic shown in the inset, the device with optimal nitrogen incorporation presents a better immunity against PBTI stress in terms of high-k trap generation.
- Fig. 4.19 Comparison of I_d degradation between “optimal” and “control.” The optimal samples show a lower initial trap density and better stress immunity (i.e., a larger τ_c).
- Fig. 4.20 Stress temperature effect on I_d degradation rate in the “optimal” sample. The cross-over is still observed, indicating the existence of two-stage degradation.

Chapter 5

- Fig. 5.1 NBTI degradation measured by using a conventional method and by using the transient measurement system described in Chapter 2. The transient measurement technique retrieves significant amount of I_d instability and anomalous characteristics.
- Fig. 5.2 The pulse trains applied to gate and drain.
- Fig. 5.3 Stress V_g dependence of NBT stress induced drain current change. Anomalous current enhancement during the initial stage of stressing and a turn-around behavior are observed for high $|V_g'|$.
- Fig. 5.4 Stress temperature dependence of NBT stress induced drain current change. Anomalous turn-around is also observed for high T.
- Fig. 5.5 Stress V_g effect at different stages of stressing. For short stress durations (0.1s, 10s), a concave-up V_g dependence is observed. For prolonged stressing (1000s), the trend evolves to that as expected, or higher $|V_g|$ induces worse degradation.
- Fig. 5.6 Stress temperature effect at different stages of stressing. While for a short stress duration (10s) $\Delta I_{d,lin}$ changes from degradation for low T to

enhancement for high T, a long stressing period (1000s) gives a trend as expected, or a higher T induces worse degradation.

Fig. 5.7 Energy band diagram at equilibrium (a), for a low stress $|V_g|$ (b), and for a high stress $|V_g|$ (c). ΔE_t denotes the available trap sites in high-k readily for trapping valence electrons from the poly-gate, and increases significantly for a high stress $|V_g|$.

Fig. 5.8 Recovery transient I_d in small area devices for short stress time (0.2s) for a low $|V_g|$ (-1.5V) (a), and for a high $|V_g|$ (-2.2V). Discontinuous current changes represent charge escape from dielectric traps, revealing the charge species injected during stress. An upward jump corresponds to a single hole charge, and a downward shift to a single electron. For the low $|V_g|$ case, only two holes are trapped during stress, while for the high $|V_g|$ case both electrons and holes are introduced into dielectric traps during stress.

Fig. 5.9 A schematic diagram illustrating the bias conditions for charge pumping measurement in a pMOSFET.

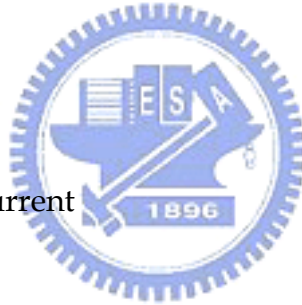
Fig. 5.10 Charge pumping measurement before and after stress. The effect of stress $|V_g|$ is indicated in (a). Impact of high-k integrity is compared in (b).

Fig. 5.11 Impact of high-k integrity on ΔI_d behavior. High-k integrity determines the polarity of ΔI_d .

Fig. 5.12 Even for a stress time long as 1000s, the V_g dependence still exhibits a turn-around feature, as opposed to that for an optimal device as indicated in Fig. 5.5.

LIST OF SYMBOLS

C_{db}	Drain-to-bulk capacitance
C_{gd}	Gate-to-drain capacitance
C_p	Parasitic capacitance
$C(x_i)$	Capacitance for trapped charges located at x_i from high-k/IL interface
D_{it}	Interface trap density
E_a	Trap activation energy
E_t	Trap energy (from the conduction band)
f_c	Fermi-Dirac distribution function
G_m	Transconductance
k	Boltzmann constant
I	Current
I_b	Bulk current
I_d	Drain current
I_e	Electron current
I_h	Hole current
I_{sd}	Source/Drain current
L	Gate length
L_{eff}	Effective gate length
m_0	Free electron mass
m^*_k	Electron effective mass in high-k
$m^*_{ox,e}$	Hole effective mass in high-k
$m^*_{ox,h}$	Hole effective mass in SiO ₂
N_C	Effective density of states in the Si conduction band
N_{HK}	Volume high-k trap density
N^V_{HK}	Area high-k trap density
N_t	Trap density
Q	Trapped electron density
q	Electronic charge
T	Temperature
T_{HK}	Physical thickness of a high-k layer



T_{ox}	Physical thickness of a SiO_2 layer
t	Time
t_{BD}	Time-to-breakdown
t_{meas}	Measurement time
t_{stress}	Stress time
V	Voltage
V_d (V_D)	Drain voltage
$V_{d,\text{meas}}$	Measurement drain voltage
$V_{d,\text{stress}}$	Stress drain voltage
V_g (V_G)	Gate voltage
V_{gh}	High-level gate voltage for charge pumping measurement
V_{gl}	Low-level gate voltage for charge pumping measurement
$V_{g,\text{meas}}$	Measurement gate voltage
$V_{g,\text{stress}}$	Stress gate voltage
V_t	Threshold voltage
W	Channel width
$\overline{x_{\text{eff}}}$	Effective distance of trapped charges from high-k/IL interface
x_i	Distance of the i^{th} trapped charge from high-k/IL interface
\hbar	Reduced Planck constant
ΔE_t (ΔE)	Energy range for dielectric traps of interest
ΔG_m	Change in transconductance
ΔI_d	Change in drain current
$\Delta I_{d,\text{lin}}$	Change in linear drain current
ΔV_t	Change in threshold voltage
Φ_B	High-k/ SiO_2 conduction band offset
α_k	Coefficient of tunneling probability through high-k
α_{ox}	Coefficient of tunneling probability through SiO_2
ϵ_{HK}	Dielectric constant of high-k gate dielectric
μ_n	Electron mobility
ν	Attempt-to-escape frequency
σ_0	Trap cross section

τ_c	Corner time for the two stage PBTI drain current degradation
τ_i	The i^{th} trapped charge emission time
τ_0	Characteristic time for tunneling
v_{th}	Thermal velocity

